Title

The developmental basis for scaling of mammalian tooth size

Journal

Proceedings of the National Academy of Sciences of the United States of America, 120(25)

ISSN

0027-8424

Authors

Christensen, Mona M
Hallikas, Outi
Roy, Rishi Das
et al.

Publication Date

2023-06-20

DOI

10.1073/pnas.2300374120

Peer reviewed

PNAS RESEARCH ARTICLE | DEVELOPMENTAL BIOLOGY

The developmental basis for scaling of mammalian tooth size

Mona M. Christensen[a,1], Outi Hallikas[a], Rishi Das Roy[a], Vilma Väänänen[a], Otto E. Stenberg[a], Teemu J. Häkkinen[b,c], Jean-Christophe François[d], Robert J. Asher[e], Ophir D. Klein[b,c,f], Martin Holzenberger[d], and Jukka Jernvall[a,g,1]

Edited by Neil Shubin, The University of Chicago, Chicago, IL; received January 9, 2023; accepted May 2, 2023

When evolution leads to differences in body size, organs generally scale along. A well-known example of the tight relationship between organ and body size is the scaling of mammalian molar teeth. To investigate how teeth scale during development and evolution, we compared molar development from initiation through final size in the mouse and the rat. Whereas the linear dimensions of the rat molars are twice that of the mouse molars, their shapes are largely the same. Here, we focus on the first lower molars that are considered the most reliable dental proxy for size-related patterns due to their low within-species variability. We found that scaling of the molars starts early, and that the rat molar is patterned equally as fast but in a larger size than the mouse molar. Using transcriptomics, we discovered that a known regulator of body size, insulin-like growth factor 1 (*Igf1*), is more highly expressed in the rat molars compared to the mouse molars. Ex vivo and in vivo mouse models demonstrated that modulation of the IGF pathway reproduces several aspects of the observed scaling process. Furthermore, analysis of IGF1-treated mouse molars and computational modeling indicate that IGF signaling scales teeth by simultaneously enhancing growth and by inhibiting the cusp-patterning program, thereby providing a relatively simple mechanism for scaling teeth during development and evolution. Finally, comparative data from shrews to elephants suggest that this scaling mechanism regulates the minimum tooth size possible, as well as the patterning potential of large teeth.

scaling | size | shape | teeth | IGF

Body size evolution causes fundamental changes in an organism's ecology and physiology (1). Changes in body size have been well documented for multiple taxonomic groups (2), and these changes in overall size are typically tightly linked to the scaling of individual body parts and organs (3). The mammalian molar tooth is an example of an organ that scales with body size. This scaling link is so strong that, within evolutionary lineages, highly accurate estimates of body size can be made from simple linear measures of molar teeth (3, 4). The use of linear measurements to estimate body size is made possible by the relatively shape-invariant scaling of molars within mammalian lineages (3–5). As a result, the fossil record of molars forms much of the basis for the reconstructions of the body size dynamics in mammalian evolution (6–10).

Despite an increasing understanding of the molecular mechanisms of shape and overall size regulation (11–14), it remains unknown how evolutionary changes in organ size are achieved while keeping shape and proportions constant. Given the central role of mammalian molars in estimating body size, we set out to investigate how the shape-invariant scaling is realized during tooth development. We took advantage of the fact that two mammalian species used in developmental research, the mouse (*Mus musculus*) and the rat (*Rattus norvegicus*), provide an example of divergent body and molar tooth size but relatively similar molar tooth shape (Fig. 1*A*). This shape-invariant scaling allows us to focus on size alone, without the pervasive effects of shape differences during development (15). Another opportune aspect for our study is the first lower molar (Fig. 1*A*) being a common focus of developmental biology research on teeth. This tooth is also the preferred dental proxy for size-related patterns in paleontological research due to its low within-species variability (6).

Results

Molar Scaling Begins during the Placode Stage. As a first step, we established when the size differences between mouse and rat molars begin to appear during development. Specifically, we asked whether size differences become visible already during the patterning of cusps, or whether rat molars achieve their larger size through growth after patterning (Fig. 1*B*). Whereas the patterning process of mammalian teeth is well known to integrate inductive signaling and growth (16), it is not known whether and how scaling might be involved.

Significance

Although mammalian teeth are well known to evolve with body size, the developmental basis for tooth scaling remains poorly understood. Because organs differing only in size but not in shape are informative about scaling, we compared molar development of the mouse and the rat. Here, we show that size differences emerge gradually, beginning before the sensitive patterning period of tooth development. Gene expressions, experiments, and computational modeling reveal that insulin-like growth factor (IGF) signaling scales tooth size without perturbing the shape. This shape-invariant scaling is achieved by inverse regulation of growth and patterning genes, thereby providing a mechanism for organ scaling. Data from shrews to elephants suggest conservation of the scaling mechanism and increased patterning potential in large teeth.

Preprint: https://www.biorxiv.org/content/10.1101/2022.12.03.518730v1.

Author contributions: M.M.C. and J.J. designed research; M.M.C., O.H., R.D.R., V.V., O.E.S., T.J.H., J.-C.F., and R.J.A. performed research; R.D.R., T.J.H., J.-C.F., R.J.A., O.D.K., and M.H. contributed new reagents/analytic tools; M.M.C., O.H., R.D.R., M.H., and J.J. analyzed data; and M.M.C. and J.J. wrote the paper with input from all authors.

The authors declare no competing interest.

This article is a PNAS Direct Submission.

[1]To whom correspondence may be addressed. Email: mona.christensen@helsinki.fi or jernvall@fastmail.fm.

This article contains supporting information online at https://www.pnas.org/lookup/suppl/doi:10.1073/pnas.2300374120/-/DCSupplemental.

Published June 12, 2023.

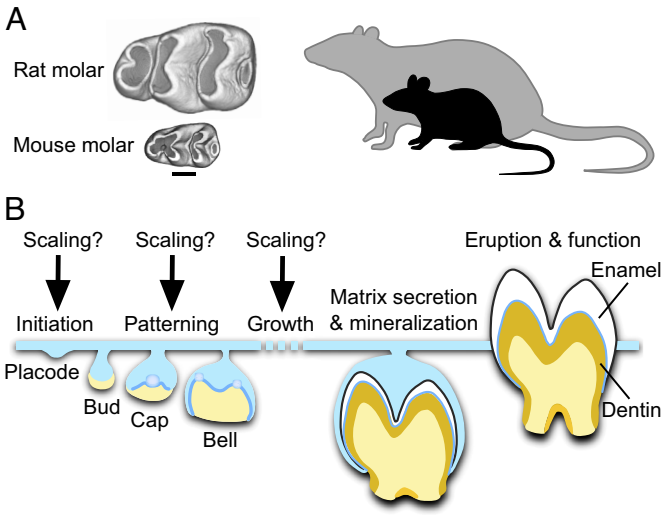

Fig. 1. Determining when teeth are scaled during development. (*A*) First lower molars of the mouse and the rat are similar in overall shape, but the rat molar is two times larger in linear dimensions. This reflects the body size difference between the species. Occlusal views of μCT reconstructed molars, anterior to the left, buccal to the top. (Scale bar for teeth, 500 μm.) (*B*) When and how during tooth development the scaling process occurs is not known. Tooth development is regulated by the interactions between the epithelial (blue) and mesenchymal (yellow) tissues. After mineralization and eruption, crown shape cannot be remodeled.

To pinpoint the onset of scaling, we compared molar development of the mouse and the rat chronologically by starting from the dental placodes. These are the earliest individualized dental structures to form when the epithelium begins to invaginate into the underlying mesenchyme. Because it is difficult to reliably delineate the size of the epithelial placode morphologically, we used in situ hybridization to detect gene expression of two epithelial markers, forkhead box I3 (*Foxi3*) and sonic hedgehog (*Shh*). *Foxi3* expression encompasses the entire placodal epithelium (17), and *Shh* is expressed within the placode in the early signaling centers, the initiation knots (18).

When multiple placodes are examined, *Foxi3* expression domains overlap in size between the mouse and the rat (P = 0.1626, all P-values determined using two-tailed randomization test, Fig. 2*A* and *SI Appendix*, Table S1). This suggests that the overall sizes of the placodal epithelia are similar in the species. However, the *Shh* expression domain, which is up-regulated within the placode in the initiation knot (18), is slightly larger in the rat than in the mouse (P = 0.0008, Fig. 2*B* and *SI Appendix*, Table S1). Formation of the initiation knot marks the beginning of the transition from placode to bud stage, and this step appears to also mark the beginning of scaling.

Examining the expression patterns in more detail shows that the size difference between the mouse and rat is driven by an increasing difference along the longitudinal axis (*SI Appendix*, Table S1). This difference becomes more pronounced when the primary enamel knot appears 2 d after the placode stage in both species (embryonic days E14 and E16 in the mouse and the rat, respectively). The primary enamel knot is an epithelial signaling center that forms toward the end of the bud stage when the invaginated epithelial bud starts to grow lateral folds called the cervical loops. Cervical loop growth marks the onset of the cap stage, during which tooth crown morphogenesis begins. The rat primary enamel knot, detected with *Shh* expression, is roughly twice as large in area as that of the mouse (Fig. 2*C* and *SI Appendix*, Table S1), suggesting a marked difference in signaling activity between the species at the onset of crown formation. Overall, scaling of tooth size appears to start before the active patterning of cusps.

Molar Scaling Encompasses All the Patterning Stages. To examine whether scaling is a significant factor affecting growth during patterning, we analyzed developing crown morphologies. From the cap stage onward, size measurements can be carried out using three-dimensional (3D) reconstructions. We used soft-tissue μCT (microcomputed tomography) imaging to reconstruct both the size and shape of the growing molars (*Materials and Methods*). To quantify the overall progression of patterning in which individual cusps become gradually identifiable, we used orientation patch count (OPC) to measure surface complexity (19).

Aligning the growth series of mouse and rat molars based on days after placode initiation makes it apparent that rat molars grow substantially faster (Fig. 3*A*). When plotted (using mm^2, Fig. 3*B* and *SI Appendix*, Table S2), both molars appear to achieve their final sizes within about 10 d after the placode stage. Logistic growth models fitted to the data suggest that the inflection points, after which the growth begins to slow down, occur close to 7 d after the placode stage (days E19 and E21 for the mouse and rat, respectively, Fig. 3*B*). Considering that the stage with the final number of main cusps is separated by 7 d from the placode stage in both species (Fig. 3*A*), scaling appears to encompass all the stages of cusp patterning. Indeed, in contrast to the pronounced differences in size, OPC values show largely similar increases of topographic complexity in the two species (Fig. 3 *C* and *D* and *SI Appendix*, Table S2). The slightly higher OPC values of the rat molar reflect its more distinct anterior part of the crown (anteroconid) and an additional distobuccal cusp (arrowheads in Fig. 3*A*). The inflection points of increase in complexity precede those of the increase in size by 2.5 and 1.4 d for the mouse and rat, respectively (Fig. 3*D*), further indicating that patterning is embedded within the scaling process of teeth.

Taken together, these results point to largely comparable rates of shape development between the mouse and the rat molars, although the teeth themselves increase in size at very different rates. A major implication of this observation is that the patterning

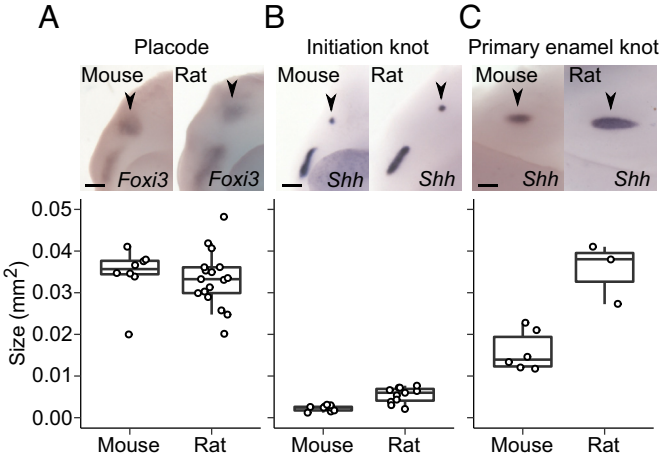

Fig. 2. Tooth scaling begins during the placode stage of molar development. (*A*) The epithelial placodes (black arrowheads) are similar in size in the rat (n = 17) and mouse molar, visualized using *Foxi3* expression (n = 8, randomization test P = 0.1626). (*B*) The initiation knots (black arrowheads, visualized using *Shh* expression) are larger in the rat (n = 11) than in the mouse (n = 9, P = 0.0008). (*C*) The primary enamel knots (black arrowheads, visualized using *Shh* expression) are larger in the rat (n = 3) than in the mouse (n = 6, P = 0.0131). Boxes enclose 50% of observations, the horizontal bar denotes the median, and whiskers extend to last values within 1.5 interquartiles. For the images, anterior is to the left, buccal to the top. (Scale bars, 200 μm.)

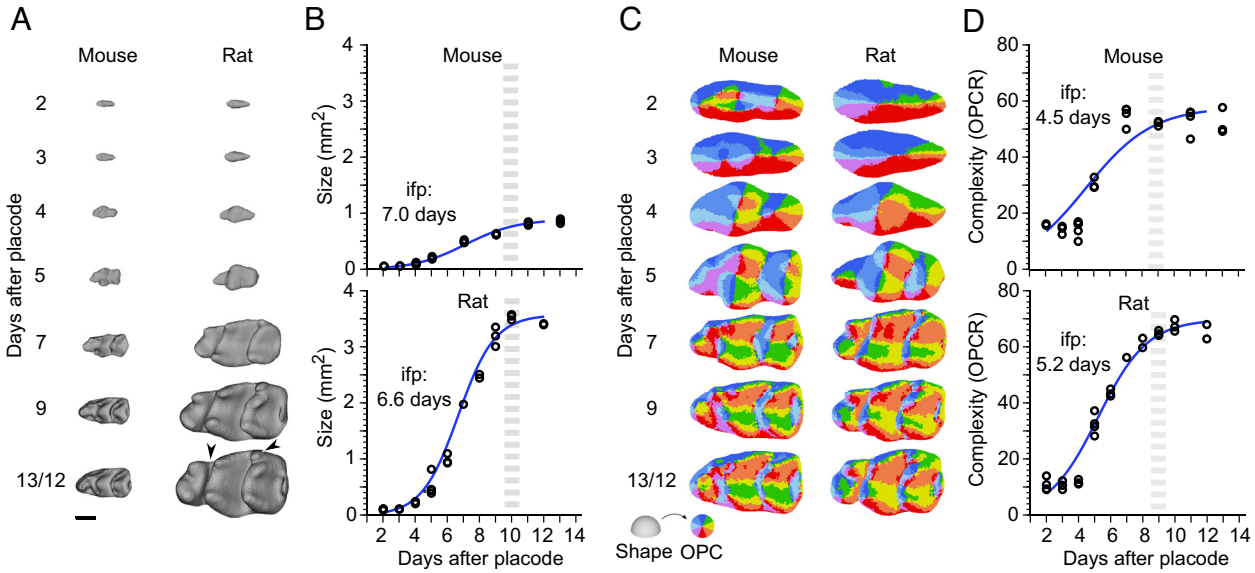

Fig. 3. Despite accelerated growth in size, rat molar patterning is similar to mouse molar patterning. (*A*) Three-dimensional (3D) reconstructions show rat molars becoming progressively larger throughout development (n = 26 and 28 for mice and rats, respectively). (*B*) Despite the much faster growth of the rat molar, logistic curves fitted to the areas indicate comparable time points for the onset of growth deceleration (inflection point, ifp) and reaching of the final tooth size (gray dashed line). For logistic curve to calculate the size $S(t) = K/1+Ae^{-kt}$; *K, A,* and *k* are 0.9, 80.9, and 0.62 for the mouse, and 33.6, 350, and 0.88 for the rat, respectively. (*C*) OPC maps of dental complexity show generally comparable progression of patterning. (*D*) Compared to the size, logistic curves fitted to the OPCR values are relatively similar between the species, the inflection point being slightly earlier in the mouse. For logistic curve to calculate the OPC $O(t) = K/1+Ae^{-kt}$; *K, A,* and *k* are 57.8, 8.6, and 0.48 for the mouse, and 69.8, 29.6, and 0.65 for the rat, respectively. The higher OPCR values of the rat molar reflect its more distinct anteroconid and an additional distobuccal cusp, arrowheads in *A*. Anterior to the left, buccal to the top. (Scale bar, 500 μm in *A*.)

happens in tissue domains that differ in size. This in turn indicates that the patterning process itself scales.

Scaling of Patterning Involves Changes in the Spacing of Signaling Centers. The morphological appearance of cusps is preceded up to 1 d by the formation of transient signaling centers, called the secondary enamel knots, that differentiate at the locations of the future cusps (15, 20). Because the OPC analysis shows that patterning occurs in larger size in the rat (Fig. 3), we used the expression of fibroblast growth factor 4 (*Fgf4*) to examine whether the spacing of the secondary enamel knots also differs between the mouse and rat (Fig. 4*A*). The results confirm that during the patterning stage the rat molar is not only larger than the mouse molar, but also that the secondary enamel knots are more spread apart ($P = 0.0001$ for both size and patterning, Fig. 4 *A* and *B* and *SI Appendix*, Table S3). Thus, the scaling of tooth size appears to be linked to the dynamics of patterning regulation, and not, for example, to cell size differences between the species (*SI Appendix*, Fig. S1).

Modifying IGF1 (Insulin-like Growth Factor 1) Signaling Is Sufficient to Scale both Size and Patterning. Next, we examined how signaling and regulation of proliferation are integrated to scale teeth. To identify molecular mechanisms that could explain the scaling of both tooth size and patterning, we first used RNA sequencing (RNAseq) to compare gene expression between the two species. We performed RNAseq analyses for mouse and rat molars that were 1, 3, and 4 d from the placode stage (corresponding to bud, late cap, and bell stages, *Materials and Methods*). Although the overall expression levels of genes required for normal tooth development are highly comparable between the species (21), we found that many genes of the insulin-like growth factor (*Igf*) pathway were expressed at higher levels in the rat than in the mouse molar (Fig. 5*A* and *SI Appendix*, Table S4). In particular, *Igf1* was consistently expressed at much higher levels in the rat (Fig. 5*A* and *SI Appendix*, Table S4), and *Igf2,* which also functions through the IGF1 receptor, showed higher expression levels in the later stages of the rat molar development (*SI Appendix*, Table S4). Moreover, several of the genes encoding IGF-binding proteins that modulate local IGF1 signaling were highly expressed in the rat molar (*SI Appendix*, Table S4). The IGF1 receptor–mediated pathway is required for various aspects of tissue growth, such as proliferation and survival (22, 23), and it is well established as a regulator of body size in dogs, humans, and mice (24–26). Whereas IGF1 functions postnatally mainly as a liver-derived endocrine hormone (25), the expression of *Igf1, Igf2,* and their receptor *Igf1r* in developing teeth [(27), *SI Appendix*, Table S4] suggests a paracrine involvement of IGF signaling in tooth size regulation. Later during tooth development, IGF signaling is

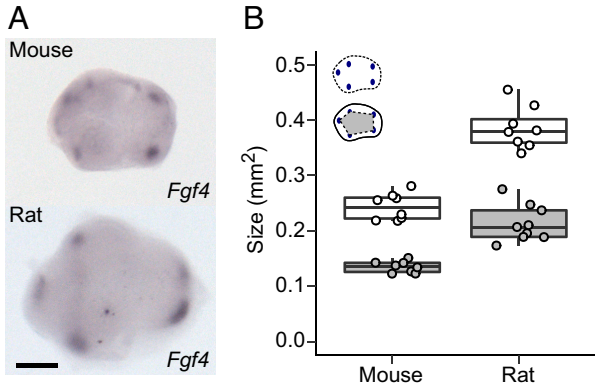

Fig. 4. Scaling of patterning involves changes in tooth size and spacing of signaling centers. (*A*) Secondary enamel knots visualized using in situ hybridization of *Fgf4* expression in the mouse and rat molar. (*B*) The rat molar is larger (size shown with white points, n = 8), and the secondary enamel knots are more spread apart (patterning area shown with gray points, n = 9) than in the mouse molar (n = 8 for both measurements). All *P*-values are 0.0001. Boxes enclose 50% of observations, the horizontal bar denotes the median, and whiskers extend to last values within 1.5 interquartiles. Anterior to the left, buccal to the top. (Scale bar, 200 μm.)

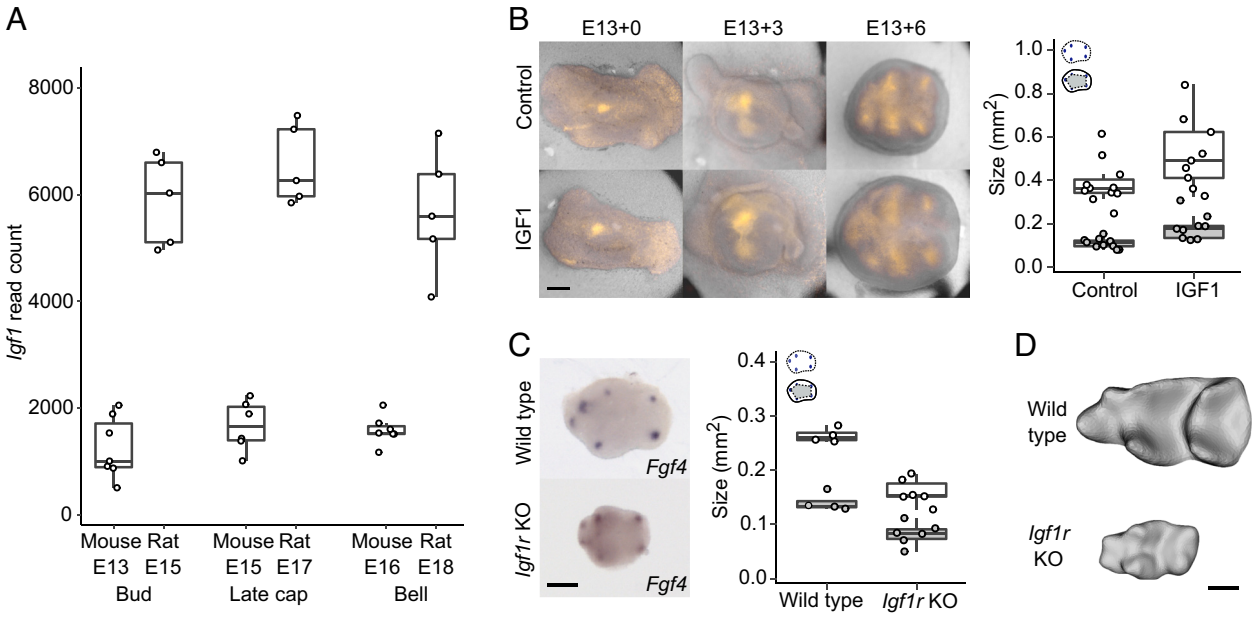

Fig. 5. Modifying IGF1 signaling is sufficient to scale both tooth size and cusp patterning. (*A*) *Igf1* is up-regulated in the rat molars (n = 5 for all stages) compared to mouse molars (n = 7 per stage except late cap stage n = 6). (*B*) IGF1-treated molars are larger (n = 9, $P = 0.0339$) and have more spread of secondary enamel knots ex vivo (n = 9, $P = 0.0001$) than those of the controls (n = 11 for both measurements). (*C*) *Igf1r* KO mouse molars are smaller (E18, n = 6, $P < 0.0045$) and their secondary enamel knots are less spread (n = 6, $P < 0.0055$) than those of wild-type mouse molars (E17, n = 4). (*D*) Wild-type and *Igf1r* KO mouse molars at E19 when all the main cusps are visible. Boxes enclose 50% of observations, the horizontal bar denotes the median, and whiskers extend to last values within 1.5 interquartiles. Anterior to the left, buccal to the top. (Scale bars, 200 μm.)

also important for tooth attachment to the jaw, as it regulates periodontal ligament formation (28).

To analyze the effects of IGF signaling on molar development experimentally, we first tested whether the IGF1 protein is capable of scaling up mouse molars ex vivo. IGF1 has been reported to increase tooth size in cultured or bioengineered molars (29, 30), but its effects on normal patterning of enamel knots and cusps have not been studied. To visualize cusp patterning in culture, we used Fucci-red cell-cycle reporter mice and cultured their molars from bud stage (E13.5) with or without recombinant IGF1 protein (*Materials and Methods*). As the secondary enamel knots are non-proliferative, they become visible in Fucci-red mice before differentiation of the rest of the crown. We found that the size of IGF1-treated teeth is 35% larger on average than that of the controls ($P = 0.0339$, Fig. 5*B* and *SI Appendix*, Table S5). Similarly, the spacing of the secondary enamel knots of the treated teeth has increased in unison with the tooth size ($P < 0.0001$, Fig. 5*B* and *SI Appendix*, Table S5), suggesting that excess IGF1 can both increase tooth size and scale the patterning so that the shape remains the same.

To examine how dependent tooth development is on canonical IGF signaling, we used an in vivo model of the *Igf1r* knockout (*Igf1r*-KO) mouse (31). Because these mice die perinatally, we analyzed the embryonic development of the molars (*Materials and Methods*). *Fgf4* expression in bell-stage molars showed reduced spacing of the secondary enamel knots ($P = 0.0055$), as well as reduced tooth size, in the *Igf1r*-KO molars ($P = 0.0045$, Fig. 5*C* and *SI Appendix*, Table S6), suggesting that the patterning process is downscaled in the mutant teeth. At E19, the *Igf1r*-KO molars have acquired all the main cusps even though they are only 33% in size of the E19 molars of wild-type mouse (Fig. 5*D*).

Taken together, IGF signaling appears to be sufficient to change both the size of the tooth and the patterning process, which in combination provides a mechanism for shape-invariant scaling. This inference raises the question of how IGF1 affects induction of secondary enamel knots, because the characteristic roles of IGF signaling are associated with growth and metabolism (22, 23), not patterning.

IGF1 Inhibits the Expression of Genes Required for Cusp Patterning. To identify the downstream effects of IGF1 signaling in teeth, we treated cap-stage (E14) mouse lower molars with recombinant IGF1 protein for 6 h (*Materials and Methods*) followed by RNAseq analysis of differential gene expression. The IGF1 treatment shows the expected bias toward upregulation of metabolic and biosynthesis-related genes (*SI Appendix*, Fig. S2*A*), whereas the down-regulated genes appear to be related to developmental regulation (*SI Appendix*, Fig. S2*B*). A closer examination of these results shows that several DNA replication markers were up-regulated by IGF1 (Fig. 6*A*), implicating the stimulation of cell proliferation. In strong contrast, there was a total lack of upregulation of any of the known developmental genes (21) required for normal tooth morphogenesis (Fig. 6*B* and *SI Appendix*, Table S7). Instead, we found eight tooth genes to be down-regulated ($P < 0.05$, Fig. 6*B* and *SI Appendix*, Table S7), five of which are expressed in the enamel knots. Of the down-regulated genes, *Lef1* and *Bmp4* are required for the induction of the molar enamel knots (32, 33), while the others alter cusp patterns when mutated (21). Overall, IGF signaling appears to have a dual role in tooth development: induction of growth and, at the same time, inhibition of cusp patterning. This result may also help to explain why attempts to increase tooth size experimentally by increasing tissue size or by recombining tissues lead to an increase in cusp number (34, 35). It is conceivable that our results on the mouse apply to humans because teeth of patients with Laron syndrome, which causes IGF1 deficiency, have been reported to have normal morphology despite reduction in size (36). Furthermore, the enlarged teeth of an IGF1-treated leprechaunism patient (37) appear at least superficially fairly normal in shape.

To further investigate the principle of dual requirement of growth and patterning regulating scaling, we used a computational model of tooth development to scale teeth [ToothMaker, (16)]. This

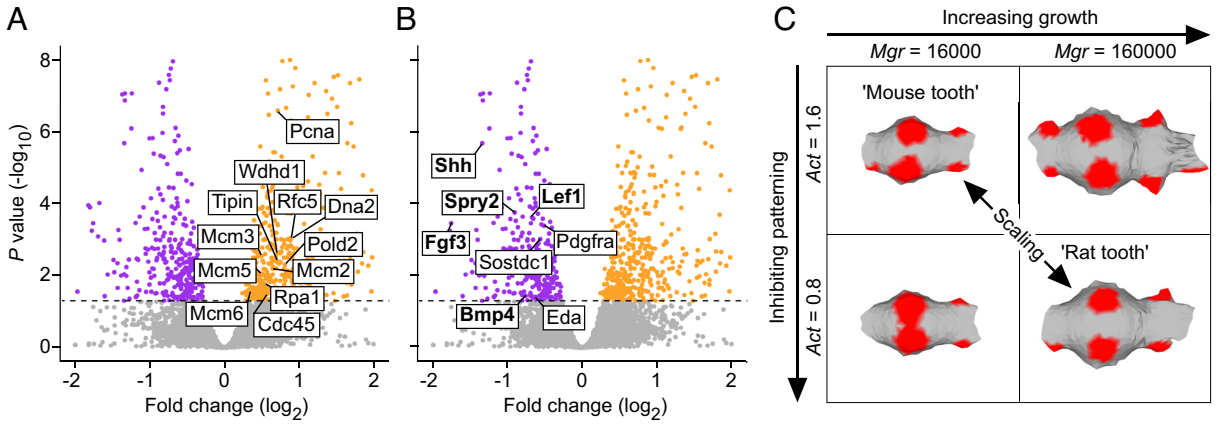

Fig. 6. Simultaneous promotion of overall growth and inhibition of cusp patterning by IGF1 provides a mechanism to scale teeth. (*A*) Mouse molars treated with IGF1 protein for 6 h show upregulation (orange) of 12 DNA replication markers (GO:0006260), n = 5 for both the treatments and controls. (*B*) In contrast to growth-promoting effects (*A*), genes required for normal tooth development show only downregulation in IGF1-treated molars (down-regulated genes in purple). Enamel knot expressed genes are in bold. Horizontal line denotes P_{adj} = 0.05. Volcano plots are zoomed to the genes of interest, see *SI Appendix*, Fig. S2, for the overall fold enrichment of GO categories. (*C*) Computer simulations of molar development using ToothMaker show that changing proliferation rate (*Mgr*) or activator autoregulation (*Act*) alone changes the pattern (forming secondary enamel knot regions shown in red). By increasing growth and by decreasing activation, which mimic the effects in *A* and *B*, the simulated mouse tooth can be scaled up. See text and *Materials and Methods* for details.

morphodynamic model integrates signaling and tissue growth to simulate tooth development, and it has been used in experimental and evolutionary studies (16, 38–42), but not to examine scaling. As a starting point, we used the simulated mouse molar from previous studies (16, 38) and increased its size (*Materials and Methods*). Increasing only the growth resulted in additional secondary enamel knots and altered cusp pattern (Fig. 6*C* and *SI Appendix*, Table S8). However, by simultaneously decreasing the activator required for enamel knot induction, we obtained a larger tooth that retains the mouse pattern with more widely spread enamel knots (Fig. 6*C* and *SI Appendix*, Table S8). Decreasing activation resulted in the requirement of a larger number of activator-producing cells, hence larger size, to reach the threshold to induce the secondary enamel knots. Taken together, we interpret these results to support the role of IGF signaling, likely through changes in many of the pathway genes (*SI Appendix*, Table S4), as a single "dial" that simultaneously promotes growth and inhibits patterning.

Comparative Data on Mammalian Teeth Support Universality of the Scaling Mechanism. Because our inferences on the scaling of patterning were based on two murine species, we wanted to examine a broader range of species and sizes. Here, we took advantage of our observation that differences in tooth width between the mouse and rat appear to become discernable relatively late, beginning with the cap stage (Fig. 3*A* and *SI Appendix*, Tables S1 and S2). Frontal histological sections of cap-stage teeth are available for different species in the literature as also in museum collections, providing data to use tooth width as a proxy for tooth size (Fig. 7*A* and *SI Appendix*, Table S9). We therefore measured early cap-stage and corresponding fully formed tooth widths of 14 mammalian species, ranging in size from the shrew (*Sorex araneus*) to the elephant (*Loxodonta africana*) (*SI Appendix*, Table S9). The measurements show that even though these teeth vary over 74-fold in final, mineralized width, the early cap-stage widths exhibit very little change in size (Fig. 7*B* and *SI Appendix*, Table S10). This means that whereas the fully formed teeth scale with body size, the early cap-stage tooth germs are relatively size invariant.

The fully formed, final tooth size can be expected to be close to the cap-stage width in single-cusped teeth when their cervical loops grow directly downward. The average width of our cap-stage measurements was 178 μm (*SI Appendix*, Table S9). Taking into account the regression slope, the extrapolated minimum width for the cap stage would be even smaller at 154 μm, suggesting this as the theoretical lower limit for tooth size in mammals (arrow at 2.2 log10 in Fig. 7*B* and *SI Appendix*, Table S10). Notwithstanding that this limit should be considered an approximation (*SI Appendix*, Table S10), it is still instructive to consider the empirical data. Experimentally, extreme reduction in tooth size has been achieved in mice with activated epithelial Wnt signaling (43). In these mice, teeth are continuously generated, typically with round, peg-like morphology (43). As the size distribution of these teeth has not been examined previously, we quantified the sizes of 42 mineralized teeth obtained from a single-molar germ transplant experiment, cultured under the kidney capsule (43). The frequency distribution of the teeth shows (*SI Appendix*, Fig. S3) that, toward the smaller teeth, their size distribution falls steeply around 200 μm, with only one tooth being clearly narrower than the predicted minimum (98 vs. 154 μm). Moreover, teeth with two

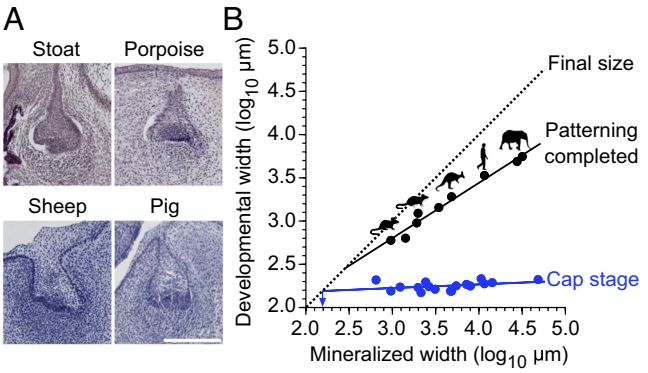

Fig. 7. Patterning scales across mammals. (*A*) Frontal sections of developing teeth of various mammals show similar buccolingual widths of tooth germs at early cap stage. The sections show dp4 (sheep), p4 (stoat), and dp3 (pig). The porpoise tooth identity cannot be determined. (*B*) The cap-stage tooth widths (blue) do not show a marked increase with the final mineralized tooth widths (regression slope is 0.043 and the intercept is 2.095, r^2 = 0.163), and the regression-line extrapolated minimum tooth width is 154 μm for single-cusped teeth (arrow). In contrast, the widths when the patterning is completed increase as the teeth become larger (black line, regression slope is 0.640 and the intercept is 0.885, r^2 = 0.976). The point when tooth development reaches the final tooth size is marked with the dashed diagonal (*X* and *Y* axis values are the same). For sample and regression details, see *SI Appendix*, Tables S9 and S10. (Scale bar, 200 μm in *A*.)

well-differentiated cusps appear to be at least about 400 μm wide (*SI Appendix*, Fig. S3).

Although the data to compare scaling of patterning are more limited, we nonetheless obtained tooth widths for seven species at the stages when the last forming cusps have just been initiated during ontogeny (*Materials and Methods* and *SI Appendix*, Table S9). Unlike the early cap-stage tooth germs, these fully patterned teeth scale with the final tooth width (Fig. 7*B*). Considering again the widths of developing teeth, the best-fit line for bell-stage teeth extrapolated toward zero overlaps with a theoretical minimum at 286 μm (2.5 log10 in Fig. 7*B* and *SI Appendix*, Table S10). This indicates that patterning is truncated in smaller teeth and agrees with the lack of teeth with second cusps in the transplant experiment (*SI Appendix*, Fig. S3). To the extent that these values are representative of mammalian tooth development in general, the downscaling capacity of teeth appears to be progressively constrained when teeth become less than half a millimeter in diameter. It is therefore interesting to contrast these extrapolations with cases of evolutionary miniaturization of mammalian teeth. Mammalian molars can be less than 500 μm in diameter, even with multiple cusps such as the mouse third molars. The smallest fossil eutherian known, *Batodonoides vanhouteni* from the Eocene, has tribosphenic lower molars that are 450 μm to 560 μm wide (44), agreeing with the minimum size for multicusped teeth. Perhaps, the smallest known mammaliaform teeth are the transversely compressed triconodont teeth of *Hadrocodium wui* from the Early Jurassic (45). These, at 230 μm to 280 μm wide, are approaching the predicted lower limit for tooth size. Moreover, the *Hadrocodium* specimen (45) has also well-preserved peg-like incisors whose diameters appear very close to the predicted 154 μm limit.

For larger teeth, the consequence of the size-invariant initiation, followed by the scaling of the patterning, is a progressive increase of growth during patterning as the teeth become larger. For example, whereas linear size in the mouse increases by 3.8 times in the cap stage relative to the end of the patterning, the comparable increase is 15.4 times in the human (calculated for 1 mm- and 10 mm-sized teeth, respectively). After patterning, the final increases in tooth sizes are 1.6 and 3.6 times for the mouse and human, which are only about 0.4 and 0.2 times the comparable increases during patterning, respectively. In other words, patterning of larger teeth encompasses an increasingly large share of the cell divisions needed to reach the final size (Fig. 7*B*).

Discussion

Evolution of tooth size has had a central role in the reconstruction of body size evolution in mammals (2–10). Also, as size affects many aspects of an animal's ecology, size changes alone are often used as a diagnostic feature to delineate species. Evolutionary changes in body size have been frequent in mammalian evolution, and tooth size seems to track these changes closely, although with a slight delay when the change is very fast [e.g., domesticated mammals (46)]. Here, we investigated how the scaling of teeth can be achieved during development. Comparisons of mouse and rat molars show that scaling is already active during the patterning phase of tooth development. Tooth patterning, which is responsible for the formation of species-specific cusp patterns, is a critical period of morphogenesis that is sensitive to mutations in many regulatory genes (21). Our experimental data and modeling results implicate IGF signaling as a mechanism for scaling both the patterning and the size. This includes the well-established role of IGF signaling in promoting growth (22, 23), and also the regulation of secondary enamel knots by inhibiting their activation (Figs. 5 and 6). This in turn would result in the requirement for a larger number of cells to reach the signaling threshold for cusp formation in larger teeth (Fig. 6*C*). More generally, our results further underscore the diverse roles that IGF signaling appears to play in developing teeth (28, 47).

One obvious question that arises from these analyses is why should scaling and patterning be integrated. One possible answer is that larger teeth retain patterning control over a progressively greater size during development (Fig. 7*B*), which in turn may minimize accumulation of harmful changes in shape caused by growth alone. Ecologically, maintaining cusp patterns while scaling tooth size should facilitate retention of proper occlusion and dietary niche when body size changes. Yet, scaling of patterning may also have an ecologically significant side effect of allowing large teeth to elaborate their cusp patterns more than small teeth. Because specialized herbivory in mammals is typically associated with relatively large body size and large, complex teeth (19, 48), scaling of tooth patterning could have been a facilitating factor in herbivorous radiations.

The predicted minimum tooth sizes with single and additional cusps (Fig. 7*B* and *SI Appendix*, Fig. S3) may be relatively close to some of the teeth in early mammaliaforms (45, 49, 50). Making even smaller teeth might require smaller cell size, or alternative mechanisms for patterning (51). Small multicusped teeth do occur in reptiles (52) and fish (53); at least in sharks, which show a large range of tooth sizes, tooth cusp patterning has been proposed to be relatively mammal like (42). Comparative data on the overall effects of IGF signaling in different vertebrate groups, while limited (54), are suggestive that an IGF-driven mechanism could scale teeth beyond mammals.

The mammalian dentition evolved from a common ancestor with relatively simple teeth lacking transverse cusps (49, 50). The subsequent transverse expansion can be considered an evolutionary novelty and a prerequisite for the acquisition of tribosphenic molars that combine slicing and crushing functions (41, 49, 50). The sequence of evolutionary changes leading to tribospheny may explain the relatively late onset of transverse expansion of molars during development (Figs. 2 and 3 and *SI Appendix*, Tables S1 and S2). This stepwise development also enables the continuing differentiation of dentitions into wide molars and narrow anterior teeth and suggests that shape-invariant scaling of teeth is not the developmental default but an actively retained scaling relationship involving all the steps of morphogenesis.

Because organs generally scale with body size, we predict that comparable scaling of patterning, possibly driven by IGF signaling, may occur in most organs. At least in the case of teeth, which have determinate growth, the final tooth size can be used to predict the proportion of patterning phase during development. Thus, in addition to being useful in inferring body size, tooth size is also informative about development.

Materials and Methods

Animals. All mouse and rat studies were approved and carried out in accordance with the guidelines of the Finnish National Animal Experimentation Board under licenses KEK16-021, KEK19-019 (mice) and KEK17-026, KEK14-026, and KEK13-014 (rats). We used wild-type outbred NMRI (Naval Medical Research Institute) mice and RccHan:Wist Wistar rats for μCT and in situ hybridization and inbred C57BL/6JOlaHsd mice and DA/HanRj rats for transcriptomics. Tissue culture experiments were carried out using Fucci mouse line expressing nuclear red (mKO-Cdt1) in G1 cell cycle phase in NMRI background (55). IGF1R-KO mice (31, 56) were kept in outbred 129S2/SvPasCrl background. Embryo age was determined based on vaginal plug appearance (embryonic day, E0). We confirmed the comparable dental stage by comparison of tooth morphology and the appearance of dental signaling centers.

µCT. Mandibles of E13-E17 mouse and E15-20 rat embryos were fixed overnight in 4% paraformaldehyde (PFA), dehydrated gradually to 70% ethanol, and stored at +4 °C. Postnatal mandibles were fixed in 4% PFA for 1 to 2 d (depending on size) and gradually dehydrated to 70% ethanol. Phosphotungstic acid (PTA) was used to increase soft-tissue contrast for µCT imaging (57). Samples were stained in 0.3% PTA (Sigma Aldrich) in 70% ethanol for 48 to 72 h at +4 °C and stored in 70% ethanol. For scanning, samples were embedded in 1% low-melting point agarose dissolved in MilliQ water. Scanning was carried out using Bruker 1272 µCT scanner with polychromatic cone beam X-ray source (Hamamatsu L11871 20, 20 to 100 kV), 11-Megapixel xiRAY X-ray CCD camera with Onsemi KAI-11002 sensor fiber-optically coupled to P43 scintillator. Embryonic samples were scanned using 0.25 mm aluminum filter at 60 kV and 166 µA. Postnatal samples were scanned using 0.5 mm aluminum filter at 70 kV and 142 µA. The voxel size used varied between 1 and 4 µm depending on the specimen size. Reconstruction was carried out using Bruker NRecon software (v. 1.6.10.1), and ring artifact correction was used when necessary. Scanning of two *Loxodonta* fetuses (University Museum of Zoology Cambridge or UMZC 2011.10.1 and UMZC 2013.7) followed PTA staining protocols in table 2 of ref. 57. Both specimens were scanned at the Cambridge Biotomography Centre on a Nikon-Xtek H-225-ST. UMZC 2013.7 was in 0.3% PTA solution for 8 wk and scanned using 0.5 to 1 mm copper filters at 140 to 142 kV and 240 to 340 µA; UMZC 2011.10.1 was in 0.3% PTA for 1 wk and scanned without a filter at 110 kV and 167 µA.

Segmentation and Tooth Measurements. Segmentation of molars was carried out using Avizo (release 9.0.1). The epithelium was segmented manually using lasso tool and the mesenchyme using brush tool. Every 3rd to 5th section was drawn and the sections in between interpolated, but the accuracy of automatic interpolation was confirmed manually in each section, and corrected when necessary. After segmentation, the binary stack was opened in Fiji (58) and smoothed using Gaussian blur 3D-tool with x, y, and z sigma of 3. A standard deviation Z-projection was taken from the occlusal side and the tooth was measured using magic wand (area) and bounding box (maximum antero–posterior length and buccolingual width). Logistic curve fitting was done with PAST (59). We report the results using two-dimensional areas because they are commonly used in evolutionary analyses, and because these were obtainable for both in vivo and ex vivo data. For measurements from histological sections, the buccolingual widths of teeth of different species were acquired from the Museum of Natural History Berlin, Germany. Histological slides were imaged using Zeiss Axioskop, Plan-Neofluar 5× objective, and Leica DFC490 camera. Additional measurements were done from the literature (*SI Appendix*, Table S9).

OPC. For OPC measurements, the segmented mesenchymes were saved as .stl surfaces using Fiji 3D viewer. The surfaces were handled in Meshlab (version 2021.10). The faces were inverted and the basal surface of the mesenchyme was removed using the Z-painting tool to limit the analysis only to the occlusal surface. Teeth were oriented, and the scan resolution differences were corrected for by dividing the original face number with ((4/x)^2) where x is the original resolution of the scan in micrometers. The acquired value was used as the target number of faces in quadric edge collapse decimation tool. The surfaces were smoothed with 50 steps using Laplacian smooth to remove segmentation artifacts and to focus on the overall surface topography, and simplified to 4,000 faces each using quadric edge collapse decimation with planar simplification weight set to one, in order to produce relatively uniform distribution of triangles. Although the use of a similar face count is used to remove the effect of size, we note that this procedure still results in smaller triangles in teeth with low relief. In our data, this does not affect the pattern of results because the relief increases similarly between the species. OPC values measured as orientation patch count rotated (OPCR) of resolution-corrected surfaces were acquired using Morphotester [v. 11.2 (60)] with a minimum patch count of 6 (roughly matching 3 pixels in raster-based OPC). Visualization was done with modified R script in molaR (61).

Probe Synthesis. For interspecies comparison, species-specific probes were designed for each marker. Probes were designed to bind the same part of the mRNA in each species. Species-specific primers used for preparing probes are listed below. cDNA (complementaryDNA) was prepared from mouse and rat embryonic molar tooth RNA (extracted using RNeasy Plus Micro kit, Qiagen, Düsseldorf, Germany). cDNA constructs were inserted in TOPO II PCR-plasmids using TOPO TA Cloning kit with chemically competent cells according to manufacturer's protocol (Thermo Fisher Scientific, Waltham, Massachusetts, USA). Prior to in vitro RNA synthesis, plasmids were extracted using Miniprep kit (Qiagen, Düsseldorf, Germany). Plasmids were linearized and probes were prepared as described by Wilkinson & Nieto (62) using digoxigenin-conjugated nucleotides (Roche, Basel, Switzerland). Sense probes were used to confirm specificity of the antisense probes. The following primers were used (forward and reverse primers are listed, respectively): CGTAAGTCCTTCACCAGCTTG and GCTGACCCCTTTAGCCTACA for mouse *Shh,* CTTAGATCCTTCACTAACTTGGTG and GCTGACCCCTTTAGCCTACA for rat *Shh,* GGAAGGGTAATTACTGGACTC and ATGAGGCTGTTGACCATGCTG for mouse *Foxi3* (63), GAAAAGGTAATTACTGGACTC and ATGAGGCTGTTGACCATGCTG for rat *Foxi3*, CAACGTGGGCATCGGATTC and CCTCATGGTAGGCGACACT for mouse *Fgf4*, and AGGCTGCGGAGACTCTACTG and GAAACTCGGTTCCCCTTCTT for rat *Fgf4*.

Whole-Mount In Situ Hybridization. Mandibles of E12-E14.5 mouse embryos and E14-E17 rat embryos were dissected for placode and primary enamel knot analysis. To be able to detect the secondary enamel knots, E16-17 mouse molars and E18-20 rat molars were separated from the mandible and the thick outer enamel epithelium was removed. All samples were fixed overnight in 4% PFA, dehydrated to 100% methanol, and stored at −20 °C. A routine in situ hybridization protocol (62) was used with the following alterations: hydrogen peroxide and glutaraldehyde were not used; proteinase K (Roche, Basel, Switzerland) was used in 7 mg/mL concentration; before prehybridization, samples were treated with acetic anhydride in 0.1 M triethanolamine for 10 min; hybridization buffer had additional 50 µg/mL yeast tRNA and 1× Denhardt's solution (Invitrogen, Waltham, Massachusetts, USA); all posthybridization washes were carried out using 5× saline-sodium citrate (SSC), 50% formamide, 0.1% Tween20, blocking; and antibody solutions had 1% Boehringer's blocking reagent (Roche, Basel, Switzerland) and 10% and 1% of goat serum. Alkaline-phosphatase-bound anti-digoxigenin antibody (11093274910, Roche, Basel, Switzerland) was used to detect the mRNA probe. Levamisole was not used in alkaline phosphatase buffer, and BM-purple (Roche, Basel, Switzerland) was used as alkaline phosphatase substrate. Samples were imaged using Zeiss Lumar V12 stereo microscope, Apolumar S 1.2× objective, and AxiocamICc1 camera.

Placode and Signaling Center Measurements. The placode area, the initiation knot area, and the primary enamel knot area were measured using Fiji (58). Samples with weak staining were excluded. When both right and left sides of the jaw were available, left side was used. The images were converted to 8-bit and pixels included in the expression area were defined as: (tissue median pixel value−expression area minimum pixel value)/2 + expression area minimum pixel value. The area enclosed by the secondary enamel knots was determined by drawing a polygon between enamel knot centers using the polygon tool in Fiji. Only teeth where at least five enamel knots were present, but without distinct development of the cusps, were measured. The tooth areas were measured using polygon tool in Fiji. Randomization test with 10,000 permutations in R (modified from ref. 64) was used to test differences between samples for the placode size, initiation knot size, primary enamel knot size, the area enclosed by the secondary enamel knots, and tooth size during patterning (Figs. 2, 4, and 5 *B* and *C*). All the *P*-values are reported as two tailed. Alternative methods to threshold the expression domains do not alter the pattern of results. Mouse strains used in controls were the same as their experimental contrasts.

Cell Size Measurements. Cell sizes of mouse and rat embryonic molars were determined by staining 6 µm-thick histological sections with DiI (Thermo Fisher Scientific, Waltham, Massachusetts, USA) and Hoechst nuclear stain (Invitrogen, Waltham, Massachusetts, USA). Sections were rehydrated gradually to RO H_2O, washed in 1× phosphate-buffered saline (PBS) + 0.3% Triton-X, and incubated in DiI (25 mg/mL in absolute ethanol stock dissolved in 1× PBS in 1:200 ratio) for 45 min. The sections were washed in 1× PBS (4 × 5 min) and incubated in 1:2,000 Hoechst for 2 h prior to mounting. The sections were imaged using Zeiss Axio Imager M2 and Axiocam HRc camera with Zeiss 40× Plan Neofluar objective. Cell perimeters were measured using lasso tool in Fiji.

Tooth Cultures. E13 mouse molars were dissected and cultured at 37 °C with 5% CO_2 using a Trowell-type organ culture as described previously (65). Media was supplemented with ascorbic acid (100 µg/mL, Sigma-Aldrich, Burlington, Massachusetts, USA) and 750 ng/mL recombinant mouse IGF1 protein (791-MG-050, Bio-Techne, Minneapolis, Minnesota, USA) in 1× PBS + 0.1% bovine serum

albumin (BSA) or similar volume of 1× PBS + 0.1% BSA in controls. Samples were imaged daily using Zeiss Lumar V12 stereo microscope, Apolumar S 1.2× objective, and AxiocamICc1 camera. A drop of media (7 µL) was added on top of each sample daily to prevent the samples from drying. The media was changed every other day. The cultures were stopped when 5 to 6 secondary enamel knots were visible. The distribution of the secondary enamel knots was defined by drawing a polygon between enamel knot centers using the polygon tool in Fiji. The tooth areas were measured using polygon tool in Fiji.

IGF1 Induction. E14 mouse molars were dissected and cultured in a hanging drop culture (65) for 6 h pair wise so that from each embryo one tooth was treated with control media and one with IGF1-containing media (media constituents and concentrations described in the previous section). Right and left sides were balanced, n = 5 for both the treatments and controls.

Transcriptomics. Wild-type tooth germs were dissected from E13, E15, and E16 mouse molars. Teeth of corresponding morphological stages were dissected from E15, E17, and E18 rats. Minimal amount of surrounding tissue was left around the tooth germ, at the same time making sure that the tooth was not damaged in the process. The tissue was immediately stored in RNAlater (Qiagen, Düsseldorf, Germany) at −80 °C for RNAseq. For RNAseq, each tooth was handled individually. Seven biological replicates were collected for mouse and five biological replicates for rat. The numbers of left and right teeth was balanced. The samples of IGF1 induction experiment were processed similarly. Samples were homogenized in TRI Reagent (Merck) using Precellys 24-homogenizer (Bertin Instruments). RNA was extracted by guanidium thiocyanate-phenol-chloroform method and purified using RNeasy Plus micro kit (Qiagen GmbH). The RNA quality of representative samples was confirmed using 2100 Bioanalyzer (Agilent). The purity of RNA was analyzed using NanoDrop (Thermo Fisher Scientific). RNA concentration was measured by Qubit 3.0 (Thermo Fisher Scientific). The cDNA libraries were prepared using Ovation Mouse RNAseq System and Ovation Rat RNAseq System (Tecan). Gene expression levels were measured using RNAseq (platforms GPL19057, Illumina NextSeq 500). The RNAseq reads of mice and rats were evaluated and bad reads were filtered out using FastQC [v. 0.11.8 (66)], AfterQC [v. 0.9.6 (67)], and Trimmomatic [v. 0.39 (68)], and ribosomal RNA was removed using Sortmerna (69). The number of remaining, good reads varied between 30M and 90M in the rat samples and 40M and 65M in the mouse samples, and 8.9M and 22.7M reads for IGF1 induction experiment. Mouse and rat reads were aligned using Salmon [v. 0.99.0 (70)] to GRCm38 (Ensembl release 100) cDNA and Rnor_6.0 (Ensembl release 99) cDNA, respectively. For mouse and rat comparison, 16,604 one-to-one orthologous genes were found between mice and rats using Ensembl Biomart tool [v. 2.50.3 (71)]. A total of 126 additional one-to-one orthologs were added using Inparanoid8 (72) in which gene pairs with bootstrap scores of 100% were selected. Only these one-to-one-orthologues found with Biomart and Inparanoid8 (version 8.0, data downloaded on June 2020) were used for further analysis. The mouse and rat output transcript IDs of Salmon were converted to mouse gene IDs using Ensembldb (73) and Tximport [v. 1.22.0 (74)], allowing comparison of mouse and rat read counts. Deseq2 [v. 1.34.0 (75)] was used to normalize the read counts by library size and composition as well as transcript length (figures and tables show normalized counts). For gene ontology (GO) term analyses of biological processes, PANTHER 17.0 (76) was used to examine up- and down-regulated genes of the IGF1 induction experiment. Fold enrichment analysis was done using PANTHER overrepresentation test (Release 20221013, GO Ontology database DOI: 10.5281/zenodo.6799722 Released 2022-07-01) with default Fisher's exact test and false discovery rate correction (77).

Computational Modeling. ToothMaker (16) was used to investigate the scaling of mouse molar simulations used in previous studies [(16, 38) and *SI Appendix*, Table S8]. The model implements experimentally inferred genetic interactions with tissue biomechanics to simulate tooth development. The logic of the model is morphodynamic (78) in that signaling regulating patterning happens concomitantly with growth. Starting from parameters used previously to simulate mouse molar development (16, 38), we systematically increased the mesenchymal proliferation rate (*Mgr*) and decreased the autoactivation of activator (*Act*). These changes simulate increases in the growth and inhibition of patterning, respectively (*SI Appendix*, Table S8). All simulations were run for the same number of iterations (14,000), which cover the development up to early bell stage (approximately 5 d after the placode stage).

Data, Materials, and Software Availability. All measurements to evaluate the conclusions are in *SI Appendix* and accession numbers for the mouse and rat transcriptome data are GEO: GSE142199 (79) and GEO: GSE158697 (80), respectively. IGF1 induction experiment accession number is GEO: GSE218338 (81). ToothMaker simulation software with the code is available at https://github.com/jernvall-lab/ToothMaker (82).

ACKNOWLEDGMENTS. We thank M. Fortelius, V. Hietakangas, J. Laakkonen, M. Mikkola, I. Salazar-Ciudad, K. Kavanagh, and members of Jernvall lab for comments and discussions on this work; N. Di-Poï and J. Laakkonen for help with comparative material; H. Suhonen for help with microCT imaging; A. Viherä, R. Savolainen, R. Murray, M. Mäkinen, O. Saarnisalo, and M. G. Varghese for technical assistance; P. Auvinen, L. Paulin, and P. Laamanen at DNA Sequencing and Genomics Laboratory; RIKEN BioResource Center through the National Bio-Resource Project of the Ministry for Education, Culture Sports, Science and Technology (MEXT), Ibaraki, Japan, for providing the Fucci mice; and P. Giere (Museum für Naturkunde, Berlin) and J. Granroth (Finnish Museum of Natural History, Helsinki) for access and help with museum collections. For access to and assistance with *Loxodonta* specimens, R.J.A. thanks F. Stansfield, L. Hautier, and the late R. T. Allen. This study was supported by the Academy of Finland, Sigrid Jusélius Foundation, and John Templeton Foundation (J.J.); by Doctoral Programme in Biomedicine (M.M.C.); and by NIDCR R01-DE027620 and R35-DE026602 (T.J.H. and O.D.K.).

Author affiliations: [a]Institute of Biotechnology, University of Helsinki, Helsinki FI-00014, Finland; [b]Department of Orofacial Sciences, University of California, San Francisco, CA 94143; [c]Program in Craniofacial Biology, University of California, San Francisco, CA 94143; [d]Sorbonne University, INSERM, Research Center Saint-Antoine, Paris 75012, France; [e]Department of Zoology, University of Cambridge, Cambridge CB2 3EJ, United Kingdom; [f]Department of Pediatrics, Cedars-Sinai Medical Center, Los Angeles, CA 90048; and [g]Department of Geosciences and Geography, University of Helsinki, Helsinki FI-00014, Finland

1. R. Peters, *The Ecological Implications of Body Size* (Cambridge University Press, 1983).
2. F. A. Smith *et al.*, Body size evolution across the Geozoic. *Annu. Rev. Earth Pl. Sc.* **44**, 1–31 (2016).
3. J. Damuth, B. J. MacFadden, *Body Size in Mammalian Paleobiology: Estimation and Biological Implications* (Cambridge University Press, 1990).
4. S. S. B. Hopkins, "Estimation of body size in fossil mammals" in *Vertebrate Paleobiology and Paleoanthropology*, D. A. Croft, S. W. Simpson, D. F. Su, Eds. (Springer, 2018), pp. 7–22.
5. L. E. Copes, G. T. Schwartz, The scale of it all: Postcanine tooth size, the taxon-level effect, and the universality of Gould's scaling law. *Paleobiology* **36**, 188–203 (2010).
6. P. D. Gingerich, Size variability of the teeth in living mammals and the diagnosis of closely related sympatric fossil species. *J. Paleontol.* **48**, 895–903 (1974).
7. P. D. Gingerich, B. H. Smith, K. Rosenberg, Allometric scaling in the dentition of primates and prediction of body weight from tooth size in fossils. *Am. J. Phys. Anthropol.* **58**, 81–100 (1982).
8. J. Alroy, Cope's rule and the dynamics of body mass evolution in North American fossil mammals. *Science* **280**, 731–734 (1998).
9. F. A. Smith *et al.*, The evolution of maximum body size of terrestrial mammals. *Science* **330**, 1216–1219 (2010).
10. A. R. D'Ambrosia, W. C. Clyde, H. C. Fricke, P. D. Gingerich, H. A. Abels, Repetitive mammalian dwarfing during ancient greenhouse warming events. *Sci. Adv.* **3**, e1601430 (2017).
11. J. Parker, Morphogens, nutrients, and the basis of organ scaling. *Evol. Dev.* **13**, 304–314 (2011).
12. L. Boulan, P. Léopold, What determines organ size during development and regeneration? *Development* **148**, 1–9 (2021).
13. S. Harmansa, T. Lecuit, Forward and feedback control mechanisms of developmental tissue growth. *Cells Dev.* **168**, 203750 (2021).
14. Z. Wu, K.-L. Guan, Hippo signaling in embryogenesis and development. *Trends Biochem. Sci.* **46**, 51–63 (2020).
15. J. Jernvall, S. V. E. Keränen, I. Thesleff, Evolutionary modification of development in mammalian teeth: Quantifying gene expression patterns and topography. *Proc. Nat. Acad. Sci. U.S.A.* **97**, 14444–14448 (2000).
16. E. Harjunmaa *et al.*, Replaying evolutionary transitions from the dental fossil record. *Nature* **512**, 44–48 (2014).
17. V. Shirokova *et al.*, Expression of Foxi3 is regulated by ectodysplasin in skin appendage placodes. *Dev. Dynam.* **242**, 593–603 (2013).
18. I. Mogollón, J. E. Moustakas-Verho, M. Niittykoski, L. Ahtiainen, The initiation knot is a signaling center required for molar tooth development. *Development* **148**, dev194597 (2021).
19. A. R. Evans, G. P. Wilson, M. Fortelius, J. Jernvall, High-level similarity of dentitions in carnivorans and rodents. *Nature* **445**, 78–81 (2007).

20. J. Jernvall, P. Kettunen, I. Karavanova, L. B. Martin, I. Thesleff, Evidence for the role of the enamel knot as a control center in mammalian tooth cusp formation: Non-dividing cells express growth stimulating *Fgf-4* gene. *Int. J. Dev. Biol.* **38**, 463–469 (1994).
21. O. Hallikas *et al.*, System-level analyses of keystone genes required for mammalian tooth development. *J. Exp. Zool. B Mol. Dev. Evol.* **336**, 7–17 (2021).
22. J. Dupont, M. Holzenberger, Biology of insulin-like growth factors in development. *Birth Defects Res. C Embryo Today Rev.* **69**, 257–271 (2003).
23. D. LeRoith, J. M. P. Holly, B. Forbes, The insulin-like growth factors: Ligands, binding proteins and receptors. *Mol. Metab.* **52**, 101245 (2021).
24. K. A. Woods, C. Camacho-Hübner, M. O. Savage, A. J. L. Clark, Intrauterine growth retardation and postnatal growth failure associated with deletion of the insulin-like growth factor I gene. *N. Engl. J. Med.* **355**, 1363–1367 (1996).
25. K. Sjögren *et al.*, Liver-derived insulin-like growth factor I (IGF-I) is the principal source of IGF-I in blood but is not required for postnatal body growth in mice. *Proc. Nat. Acad. Sci. U.S.A.* **96**, 7088–7092 (1999).
26. N. B. Sutter *et al.*, A single IGF1 allele is a major determinant of small size in dogs. *Science* **316**, 112–115 (2007).
27. B. K. Joseph, N. W. Savage, T. J. Daley, W. G. Young, In situ hybridization evidence for a paracrine/autocrine role for insulin-like growth factor-I in tooth development. *Growth Factors* **13**, 11–17 (1996).
28. J. Jing *et al.*, Spatiotemporal single-cell regulatory atlas reveals neural crest lineage diversification and cellular function during tooth morphogenesis. *Nat. Commun.* **13**, 4803 (2022).
29. W. G. Young, Comparison of the effects of growth hormone, insulin-like growth factor-I and fetal calf serum on mouse molar odontogenesis in vitro. *Arch. Oral Biol.* **40**, 789–799 (1995).
30. T. Oyanagi *et al.*, Insulin-like growth factor 1 modulates bioengineered tooth morphogenesis. *Sci. Rep.* **9**, 368 (2019).
31. M. Holzenberger *et al.*, IGF-1 receptor regulates lifespan and resistance to oxidative stress in mice. *Nature* **421**, 182–187 (2003).
32. T. Sasaki *et al.*, LEF1 is a critical epithelial survival factor during tooth morphogenesis. *Dev. Biol.* **278**, 130–143 (2005).
33. S. Jia *et al.*, Roles of Bmp4 during tooth morphogenesis and sequential tooth formation. *Development* **140**, 423–432 (2012).
34. J. Cai *et al.*, Patterning the size and number of tooth and its cusps. *Dev. Biol.* **304**, 499–507 (2007).
35. K. Ishida *et al.*, The regulation of tooth morphogenesis is associated with epithelial cell proliferation and the expression of Sonic hedgehog through epithelial–mesenchymal interactions. *Biochem. Bioph. Res. Commun.* **405**, 455–461 (2011).
36. Z. Laron, "The teeth in patients with Laron Syndrome" in *Laron Syndrome–From Man to Mouse, Lessons from Clinical and Experimental Experience*, Z. Laron, J. J. Kopchick, Eds. (Springer, 2011), pp. 213–217.
37. T. Fukunaga *et al.*, Dental and craniofacial characteristics in a patient with leprechaunism treated with insulin-like growth factor-I. *Angle Orthodontist* **78**, 745–751 (2008).
38. E. Renvoisé *et al.*, Mechanical constraint from growing jaw facilitates mammalian dental diversity. *Proc. Nat. Acad. Sci. U.S.A.* **114**, 9403–9408 (2017).
39. Y. Savriama *et al.*, Bracketing phenogenotypic limits of mammalian hybridization. *R. Soc. Open Sci.* **5**, 180903 (2018).
40. R. W. Burroughs, Phylogenetic and developmental constraints dictate the number of cusps on molars in rodents. *Sci. Rep.* **9**, 10902 (2019).
41. A. M. C. Couzens, K. E. Sears, M. Rücklin, Developmental influence on evolutionary rates and the origin of placental mammal tooth complexity. *Proc. Nat. Acad. Sci. U.S.A.* **118**, 1–10 (2021).
42. A. P. Thiery, A. S. Standing, R. L. Cooper, G. J. Fraser, An epithelial signalling centre in sharks supports homology of tooth morphogenesis in vertebrates. *Elife* **11**, e73173 (2022).
43. E. Järvinen *et al.*, Continuous tooth generation in mouse is induced by activated epithelial Wnt/beta-catenin signaling. *Proc. Nat. Acad. Sci. U.S.A.* **103**, 18627–18632 (2006).
44. J. I. Bloch, K. D. Rose, P. D. Gingerich, New species of batodonoides (Lipotyphla, Geolabididae) from the early eocene of Wyoming: Smallest known mammal? *J. Mammal.* **79**, 804–827 (1998).
45. Z. Luo, B.-A. Bhullar, A. Crompton, A. Neander, T. Rowe, Reexamination of the mandibular and dental morphology of the early Jurassic mammaliaform Hadrocodium wui. *Acta Palaeontol. Pol.* **67**, 95–113 (2022).
46. M. Clauss, L. Heck, K. Veitschegger, M. Geiger, Teeth out of proportion: Smaller horse and cattle breeds have comparatively larger teeth. *J. Exp. Zool. B Mol. Dev. Evol.* **338**, 1–14 (2022).
47. K. A. Koffi *et al.*, The role of GH/IGF axis in dento-alveolar complex from development to aging and therapeutics: A narrative review. *Cells* **10**, 1181 (2021).
48. J. Jernvall, Mammalian molar cusp patterns: Developmental mechanisms of diversity. *Acta Zool. Fenn.* **198**, 1–61 (1995).
49. Z.-X. Luo, Transformation and diversification in early mammal evolution. *Nature* **450**, 1011–1019 (2007).
50. P. G. Gill *et al.*, Dietary specializations and diversity in feeding ecology of the earliest stem mammals. *Nature* **512**, 303–305 (2014).
51. D. Larionova, H. Lesot, A. Huysseune, Miniaturization: How many cells are needed to build a tooth? *Dev. Dyn.* **250**, 1021–1035 (2021).
52. F. Lafuma, I. J. Corfe, J. Clavel, N. Di-Poï, Multiple evolutionary origins and losses of tooth complexity in squamates. *Nat. Comm.* **12**, 6001 (2021).
53. J. T. Streelman, J. F. Webb, R. C. Albertson, T. D. Kocher, The cusp of evolution and development a model of cichlid tooth shape. *Evol. Dev.* **5**, 600–608 (2003).
54. J. Lodjak, S. Verhulst, Insulin-like growth factor 1 of wild vertebrates in a life-history context. *Mol. Cell. Endocrinol.* **518**, 110978 (2020).
55. A. Sakaue-Sawano *et al.*, Visualizing spatiotemporal dynamics of multicellular cell-cycle progression. *Cell* **132**, 487–498 (2008).
56. M. Holzenberger *et al.*, A targeted partial invalidation of the insulin-like growth factor I receptor gene in mice causes a postnatal growth deficit. *Endocrinology* **141**, 2557–2566 (2000).
57. B. D. Metscher, MicroCT for developmental biology: A versatile tool for high-contrast 3D imaging at histological resolutions. *Dev. Dynam.* **238**, 632–640 (2009).
58. J. Schindelin *et al.*, Fiji: An open-source platform for biological-image analysis. *Nat. Methods* **9**, 676–682 (2012).
59. Ø. Hammer, D. A. T. Harper, P. D. Ryan, PAST: Paleontological statistics software package for education and data analysis. *Palaeontol. Electron.* **4**, 9pp (2001).
60. J. M. Winchester, MorphoTester: An open source application for morphological topographic analysis. *PLoS One* **11**, e0147649 (2016).
61. J. D. Pampush *et al.*, Introducing molaR: A new R package for quantitative topographic analysis of teeth (and other topographic surfaces). *J. Mamm. Evol.* **23**, 397–412 (2016).
62. D. G. Wilkinson, M. A. Nieto, Detection of messenger RNA by in situ hybridization to tissue sections and whole mounts. *Meth. Enzym.* **225**, 361–373 (1993).
63. T. Ohyama, A. K. Groves, Expression of mouse Foxi class genes in early craniofacial development. *Dev. Dyn.* **231**, 640–646 (2004).
64. S. Kuiper, J. Sklar, *Practicing Statistics: Guided Investigations for the Second Course* (Pearson Higher Ed., 2012).
65. K. Närhi, I. Thesleff, Oral biology, molecular techniques and applications. *Methods Mol. Biol.* **666**, 253–267 (2010).
66. S. Andrews, FastQC: A quality control tool for high throughput sequence data (Version v0.11.8, Babraham Institute, Cambridge UK, 2010), http://www.bioinformatics.babraham.ac.uk/projects/fastqc/.
67. S. Chen *et al.*, AfterQC: Automatic filtering, trimming, error removing and quality control for fastq data. *BMC Bioinform.* **18**, 80 (2017).
68. A. M. Bolger, M. Lohse, B. Usadel, Trimmomatic: A flexible trimmer for Illumina sequence data. *Bioinformatics* **30**, 2114–2120 (2014).
69. E. Kopylova, L. Noé, H. Touzet, SortMeRNA: Fast and accurate filtering of ribosomal RNAs in metatranscriptomic data. *Bioinformatics* **28**, 3211–3217 (2012).
70. R. Patro, G. Duggal, M. I. Love, R. A. Irizarry, C. Kingsford, Salmon provides fast and bias-aware quantification of transcript expression. *Nat. Methods* **14**, 417–419 (2017).
71. R. J. Kinsella *et al.*, Ensembl bioMarts: A hub for data retrieval across taxonomic space. *Database* **2011**, bar030 (2011).
72. E. L. L. Sonnhammer, G. Östlund, InParanoid 8: Orthology analysis between 273 proteomes, mostly eukaryotic. *Nucleic Acids Res.* **43**, D234–D239 (2015).
73. J. Rainer, L. Gatto, C. X. Weichenberger, ensembldb: An R package to create and use Ensembl-based annotation resources. *Bioinformatics* **35**, 3151–3153 (2019).
74. C. Soneson, M. I. Love, M. D. Robinson, Differential analyses for RNA-seq: Transcript-level estimates improve gene-level inferences. *F1000Res.* **4**, 1521 (2016).
75. M. I. Love, W. Huber, S. Anders, Moderated estimation of fold change and dispersion for RNA-seq data with DESeq2. *Genome Biol.* **15**, 550 (2014).
76. P. D. Thomas *et al.*, PANTHER: Making genome-scale phylogenetics accessible to all. *Protein Sci.* **31**, 8–22 (2022).
77. H. Mi *et al.*, Protocol update for large-scale genome and gene function analysis with the PANTHER classification system (v.14.0). *Nat. Protoc.* **14**, 703–721 (2019).
78. I. Salazar-Ciudad, J. Jernvall, A computational model of teeth and the developmental origins of morphological variation. *Nature* **464**, 583–586 (2010).
79. O. Hallikas *et al.*, Keystone genes for tooth development. *Gene Expression Omnibus*. https://www.ncbi.nlm.nih.gov/geo/query/acc.cgi?acc= GSE142199. Deposited 17 December 2019.
80. O. Hallikas *et al.*, Keystone genes for tooth development. *Gene Expression Omnibus*. https://www.ncbi.nlm.nih.gov/geo/query/acc.cgi?acc=GSE158697. Deposited 28 September 2020.
81. M. M. Christensen, O. Hallikas, R. Das Roy, J. Jernvall, IGF1 treatment of developing mouse molar. *Gene Expression Omnibus*. https://www.ncbi.nlm.nih.gov/geo/query/acc.cgi?acc=GSE218338. Deposited 18 November 2022.
82. ToothMaker, Github. https://github.com/jernvall-lab/ToothMaker. Deposited 11 April 2018.